Progress in Organic Coatings 71 (2011) 198–205

Contents lists available at ScienceDirect

Progress in Organic Coatings

journal homepage: www.elsevier.com/locate/porgcoat

Protective abilities of nanocomposite coatings containing Al_2O_3 nano-particles loaded by $CeCl_3$

S. Kozhukharov[a,*], V. Kozhukharov[a], M. Wittmar[b], M. Schem[b], M. Aslan[b], H. Caparrotti[b], M. Veith[b]

[a] University of Chemical Technology and Metallurgy 8, Kl. Okhridsky Blvd., Sofia 1756, Bulgaria
[b] INM—Leibniz Institute for New Materials, Campus D2 2, 66123 Saarbruecken, Germany

ARTICLE INFO

Article history:
Received 24 July 2010
Received in revised form 15 February 2011
Accepted 23 February 2011

Keywords:
Nanocomposites
Hybrid coatings
EIS
Corrosion durability
AA2024-T3 Al alloy

ABSTRACT

The protective ability of hybrid nano-composite oxysilane coatings, deposited via sol–gel method on AA2024-T3 – aluminium alloy, were studied by linear voltammetry (LVA) and electrochemical impedance spectroscopy (EIS) methods in 0.05 M solution of NaCl. Cerium chloride ($CeCl_3$) was incorporated as an inhibitor into a sol–gel hybrid matrix in two different routes: directly and via filled porous Al_2O_3 nano-particle aggregates with diameters up to 500 nm. The influences of the inhibitor concentration, as well as the influence of nano-particles on the barrier properties and the susceptibility against corrosion, were evaluated and EIS spectra were fitted by appropriated equivalent circuits. The values for C_{coat}, R_{coat}, C_{oxy} and R_{oxy} were achieved and their evolution over time was investigated. The investigated coatings possess highly expressed barrier properties (10^6 to 10^7 $\Omega\,cm^2$). Despite of the chloride ions inside of the matrix, some samples illustrated a significant durability of over 4000 h during exposure to the corrosion medium before first signs of corrosion appeared. The electrochemical results were compared with the neutral salt spray test. Thus, it was proved that the potential of these coatings is to be used as anticorrosive protective materials and are candidate to replace Cr(VI)-based anti-corrosion coatings.

1. Introduction

To decrease the environmental impact on construction elements, built from different metals and alloys, actions regarding corrosion protection have to be taken. In this context part of an efficient technical solution is the deposition of protective coatings, which effectively insulate the metal surface from the corrosive environment. In the last decades, because of their high anticorrosive potential, species containing Cr(VI), were generally used for the protection of different metals. Few years ago, the usage of Cr-containing materials was prohibited in the electrical and electronic industry due to their proved toxic and carcinogenic activity. The decision was initiated by the EC's directive "Restriction of Hazardous Substances" (RoHS) in 2006. Since 2007 the Cr-coatings have also been banned in the automotive industry according to the "End of Live Vehicles" (ELV) directive. These two directives have stimulated a world-wide research activity to invent new efficient and environmentally friendly substitutions of chromium compounds and other hard metals [1–3]. The oxysilane compounds, obtained by sol gel route, have appeared as perspective alternative in this scope. These compounds could be deposited on various metal substrates: galvanized steels [4,5], stainless steels [6] and magnesium alloys [7]. The siloxanes are hybrid compounds, consisting of both organic and inorganic matter. The inorganic groups stimulate the creation of strong covalent bonds with the oxide surface layer of the metal substrates. Simultaneously, the organic part renders flexibility, decreases the number of the defects, and improves the compatibility with the upper coatings' layers [8].

The oxysilane coatings made via sol–gel route have been reported [9–13] as excellent alternatives for Cr-containing coatings intended to aluminium alloys. The aluminium alloy 2024-T3 is a material with a high industrial relevance, especially in the aerospace industry, because of its significant mechanical strength [14,15]. It is however very susceptible to local corrosion [15–19]. Consequently, its industrial application is possible only after deposition of protective coatings. It is necessary to underline that the coating systems for the aircraft industry are based on the multilayer approach – coatings with a primary layer and a top-coat [8].

The oxysilane coatings stimulate the formation of supplemental Si–O–Al conversion layers, distinguished by the stable and dense interface between the sol–gel layer and the superficial native oxide film [20]. Sol–gel derived coatings exhibit the risk of non-reliable anti-corrosion protection, because of their micro-porous structure, local cracks, ruptures, and non-equality density nature [21]. Some improvements of the coatings are achieved by the addition of ZrO_2 and CeO_2 nano-particles [22,23] or their mixtures [24]. Further

* Corresponding author. Tel.: +359 899837282; fax: +359 2 8685488.
E-mail address: stephko1980@abv.bg (S. Kozhukharov).

0300-9440/$ – see front matter © 2011 Elsevier B.V. All rights reserved.
doi:10.1016/j.porgcoat.2011.02.013

Table 1
Compositions and thickness of the coatings.[a]

Comp.	Index							
	A	B	C	D	F	G	H	I
Hybrid matrix	+	+	+	+	+	+	+	+
Al_2O_3 (wt.%)	8	8	18	18	30	30	–	–
$CeCl_3$ (wt.%)	2	4	2	4	2	4	2	4
Solvent removed (g)	10.1	8.7	37.0	35.9	35.2	35.0	4.4	3.7
Average thickness (μm)	12.9	14.0	20.4	24.8	14.8	17.2	20.2	23.6

[a] The content of Al_2O_3 and $CeCl_3$ in wt.% is related to the entire sol–gel composition.

increase of the coating's efficiency is achieved by incorporation of some inhibitor substances. The cerium ions have proved to be an excellent inhibitor. The corrosion inhibition mechanism of AA2024-alloy by Ce^{3+} was examined in details by Yasakau et al. [15]. The Ce^{3+} inhibitor efficiency is a consequence of the red-ox couple Ce^{3+}/Ce^{4+} [25,26]. The Ce^{4+} ions are converted into insoluble Ce (IV) hydroxides that precipitate at the cathodic sites of a corroding alloy, blocking the corrosion process. According to Yasakau and co-authors [15] the cerium ions could be incorporated into the coatings through different strategies. The introduction of these ions directly into the sol–gel matrix deteriorates its barrier properties and accelerates the inhibitor's leaching. It was established that separation of the inhibitor from the matrix bulk is a reasonable approach. On one hand, this attempt protects the matrix from structural damages, caused by direct interactions with the inhibitor, and on the other hand, a prolonged release effect from an inhibitor carrier provider can be expected. In a previous work [27] it was established that nano-particles of porous Al_2O_3 could be successfully utilized as containers for benzotriazole, applied as an inhibitor.

The aim of the present study was to investigate oxysilane hybrid coatings, deposited on the AA2024-alloy, and to figure out the efficiency of porous Al_2O_3 nano-particles as containers for $CeCl_3$. Despite of the introduction of chloride ions into the sol–gel hybrid matrix, an astonishing high durability of the corrosion protection of the coatings was found by an evaluation of the protective ability through the linear voltammetry (LVA) and electrochemical impedance spectroscopy (EIS) methods.

2. Experimental

2.1. Preparation and deposition of the coatings

The loaded alumina nano-containers were made according to the procedure described in [27]. Shortly, alumina powder (specific surface area 111 m^2/g, AluOx C, Degussa, now Evonik, Germany) was washed with hydrochloric acid. The inhibitor was solved in water and specific amounts of alumina were added. After 10 h of stirring procedure the particles were lyophilised. For redispersion polyvinylbutyral was added together with ethanol. After 12 h of stirring and 30 min ultrasound treatment in an ice bath the redispersed particles were characterised and loading phase, after centrifugation at 20,000 rpm, was determined by the high-performance liquid chromatography (HPLC) analysis of the supernatant.

The coatings were prepared by the standard sol–gel route. The hybrid matrix was obtained from the following precursors: 2,2′-bis-(4-hydroxyphenyl)-propane (BPA, 97%, Aldrich, Germany), 3-glycidoxypropyl trimethoxysilane (GPTS, 98%, ABCR, Germany), methyltriethoxysilane (MTEOS, 98%, ABCR, Germany) and tetraethoxysilane (TEOS, 98%, ABCR, Germany) in the presence of SiO_2 nanoparticles (Levasil 300, aqueous, colloidal disperse solution of amorphous SiO_2, Bayer AG, Germany). Three solutions were prepared. In the first one MTEOS (99.5 (weight) parts), TEOS (31.1 parts), SiO_2 nanoparticles(19.4 parts), deionized water (19.4 parts) and concentrated hydrochloric acid 1 M (22.5 parts) and the inhibitor material in the specific amount calculated on the solid content. This solution was stirred for 2 h at a room temperature. The third component was a solution of BPA in isopropoxyethanol (each 57.1 parts), achieved after 2 h of stirring. Afterwards, all three solutions were mixed together and a part of the solvent was removed by the vacuum distillation method on a rotation evaporator to increase the viscosity and thus to obtained thicker coatings. Finally, methyl imidazole was added and after 10 min of stirring the coating was applied on a pre-cleaned aluminium specimen by the dip coating method (speed of withdrawal 9 mm/s). Annealing procedure was done at 120 °C for 4 h according to [28]. The compositions of the coatings, object of the present study, are summarised in Table 1. There, the additions of nano-particles and inhibitors are represented in weight percents (wt.%) from the total composition of the coatings.

2.2. Test methods and measurement conditions

The protective ability of the coatings has been assessed by electrochemical methods as follows: linear voltammetry (LVA) in potentiodynamic regime, and electrochemical impedance spectroscopy (EIS). Glass three-electrode cell was used for both methods. The model corrosive medium was 100 ml of 0.05 M NaCl solution. A part of the coated sample's surface with a defined area of 0.64 cm^2 served as working electrode. The counter electrode was platinum net with a surface area with more than 2 orders of magnitude higher than that of the working electrode. Thus, the influence of the impedance of the counter electrode was eliminated [29]. The reference electrode was a standard one Ag/AgCl – 3 M KCl, model 6.0733.100, a product of Metrohm (Netherlands). The polarization curves were acquired by a potentiostat/galvanostat PGSTAT 30/2, "AUTOLAB", product of Ecochemie – Netherlands.

LVA-measurements were performed in potentiodynamic regime with linear sweep rate of the potential, equal to 0.005 V/s, in range from −0.600 V to +0.600 V, according to the open circuit potential (OCP). It was established that at this potential's interval the reproducibility of the results is really good, and it is not influenced by the polarization of the electrodes.

The EIS measurements were performed by FRA-2 block, used as an extension unit of PGSTAT30/2 device. All spectra were obtained in frequencies interval from 10 to 2×10 Hz, distributed into seven frequencies per decade. The amplitude of the excitation signal was 100 mV. All of the measurements were performed at OCP. The mentioned value of the amplitude was selected, as a compromise between two negative tendencies, which appear at low and at very high amplitudes, respectively. It was established that when the amplitude is too low (5–6 mV), the detection of phase shift at low frequency part is quite incorrect and randomly distributed. This effect is due to the insignificant value of the currents, passing through the working electrode (in order of nano-Amperes). If the amplitude is too high, than polarization of the electrode, as well as at destruction of the coating are possible. It was established that, at signal's amplitude up to 100 mV (as the used by other authors

[30]), the reproducibility of the results is satisfying, and they correspond to the basic requirements for linearity, stability, and absence of undesirable interactions between the input and the output signals. The correspondence of the system to these requirements was checked by applying the Kramers–Kroenig test [31].

At least two electrodes (samples) from each composition have passed the electrochemical measurements. All of them were performed at room temperature and with protection of the cell against external sources of static electric fields influence, supplied by Faraday cage.

2.3. Neutral salt spray test

Salt spray test was applied on the samples according to DIN EN ISO 9227. Before exposure to the test, each specimen was scratched once in its middle part and all of the edges were covered with bee wax. The evolution of corrosion was controlled once a week. Images were taken during each examination with a digital camera.

3. Results and discussion

3.1. Voltammetric measurements

The LVA measurements are widely used for evaluation of metal and alloy corrosion. In the cases, when the metal is covered by a protective film these measurements may not give reasonable quantitative results. On one hand, the protective film could be destroyed by the currents which pass through the coating. On the other hand, the Ohmic drop originating from the bulk of the coating is always included in the values of the polarization resistance. As a result incorrect values for the corrosion current could be determined [32]. This was the reason to apply the LVA method as a comparative method only for qualitative evaluation of the coatings.

Fig. 1 shows a correlation of the potentiodynamic polarization curves of samples after 24 h (Fig. 1(a)), and 1500 h (Fig. 1(b)) durability tests performed in 0.05 M NaCl solution.

The significant difference between the curve of the bare alloy and the other tested samples is expressed in the current densities of the cathodic and anodic branches of the curves, as well as in the values of corrosion potential (Fig. 1(a)). For the reference coating (curve 1), the current value is 4 orders lower of magnitude than this of the current of the corresponding bare alloy (curve 4). Consequently, the synthesised oxysilane coatings possess highly expressed barrier ability. This ability is deteriorated, when the inhibitor $CeCl_3$ is added directly to the matrix, i.e. samples H and I in Table 1. The corresponding anodic currents (curves 2 and 3) increase with one order of magnitude, in comparison to the reference coating (curve 1). Similar negative influence of the Ce^{3+} ions was also observed by other authors [15]. We consider a relation either with deterioration of the structure of the hybrid matrix, or with partial deactivation of the inhibitor, caused by a leaching into the electrolyte, which leaves results in a less dense coating. Besides, the higher content of $CeCl_3$ involved directly into matrix, contributes to the acceleration of the pitting formation process. The last phenomenon could be registered by the sharp current increase at a defined value of the potential (pitting potential) from the anodic branch of the polarization curve (Fig. 1(b)). In the case of inorganic–organic hybrid matrix with direct addition of 4 wt.% $CeCl_3$ we observed that pitting is already occurred after 1500 h of exposure, while in the case of 2 wt.% $CeCl_3$ in the matrix it was registered, even after 1900 h of exposure. The fact that higher loaded coatings show an earlier susceptibility to corrosion than the less filled ones supports the idea of leaching inhibitor salt into the electrolyte and leaving a less dense coating. For comparable specimen we have found a very week leaching near the detection limit of an inductively coupled plasma-optical emission spectroscopy (ICP-OES) study for samples containing 4 wt.% $CeCl_3$ in [33]. This supports the idea that leaching is responsible for the performance of the samples doped only by the Ce-salt.

Alternatively, to obtain higher inhibitor concentrations in the coating, but not to destabilise the matrix by direct integration of soluble inhibitor salts, the inhibitor was incorporated into porous Al_2O_3 nano-particle agglomerates, before their introduction into the matrix (samples A–G in Table 1). A further purpose of this approach was to supply a prolonged activity of the corresponding inhibitor, as consequence of its retained release from the nano-particle agglomerates that served as nano-containers.

The present research has proved also the insignificant influence of presence of Al_2O_3 nano-particles over the barrier ability of the corresponding coatings, during the initial hours of exposure. The anodic currents of I, D and G coatings which contain 4 wt.% $CeCl_3$ are similar and weakly depend on the nano-particle's content (Fig. 2(a)). Analogical behaviour was observed for the samples with 2 wt.% $CeCl_3$, as well (not shown in the figures). In both of cases, the inhibitor is preliminary impregnated in porous Al_2O_3 nano-particles, but their amount is calculated towards the entire composition of the sol–gel coatings.

Obviously the effect of the nano-particle's content appears at a later stage of the exposure to corrosive medium, and it has a significant impact over the durability of the coatings (Fig. 2(b)). The durability was determined by the continuation of the time since the first moment of exposing of the sample until the appearance of first signs of pitting. The coating with the highest content of nano-particles (30 wt.% Al_2O_3, see Fig. 2(b), curve 4) revealed the lowest durability. For this sample, pitting formation began after 1040 h of exposure. In the case of average nano-particles content (e.g. sample C with 18 wt.% Al_2O_3), the pitting appeared after 2800 h. For the coatings with the lowest content of Al_2O_3 nano-particles the pitting was not formed even after 3000 h of exposure (sample A with 8 wt.% Al_2O_3, curve 2 shown in Fig. 2(b)). Generally, the samples, prepared by addition of 4 wt.% $CeCl_3$, reveal lower durability than those, containing 2 wt.% of the inhibitor, independent of the method of it introduction (not shown in the figures).

Regardless the fact that the polarization measurements were used only for qualitative evaluation, they undoubtedly proved that the hybrid oxysilane coatings, with both $CeCl_3$ – inhibitor and Al_2O_3 – nano-particles, show highly expressed protective ability and remarkable corrosion durability in 0.05 M NaCl solution. The expected benefit for the protection behaviour of the coatings caused by an indirect incorporation of the inhibitor salt as an additive in Al_2O_3 nano-containers, was proven by polarization experiments. The best combination of these features was found in the coatings with 2 wt.% $CeCl_3$ and 8–18 wt.% Al_2O_3 nano-particles content in the coatings A and C, respectively.

3.2. Impedance measurements

In addition to the voltammetric measurements we have applied the electrochemical impedance spectroscopy (EIS) method. It enables the possibility to clarify the physical and chemical processes, occurring at the interfaces and in the phase bulks of the system: metal/coating/electrolyte, as well as to follow the evolution of these processes.

Fig. 3 shows the evolution of the impedance spectra for coating A. The spectra for all other samples with $CeCl_3$ possessed similar shape. In the high frequency region of these spectra a completely capacitive behaviour was observed. It should be assigned to the capacitance of the coating (C_{coat}). At the average frequency part of the spectra, in a relative broad frequency band from 0.01 Hz to 10 Hz, resistive behaviour was seen, caused by the resistance of the electrolyte penetrated in the pores of the coating R_{coat}. In

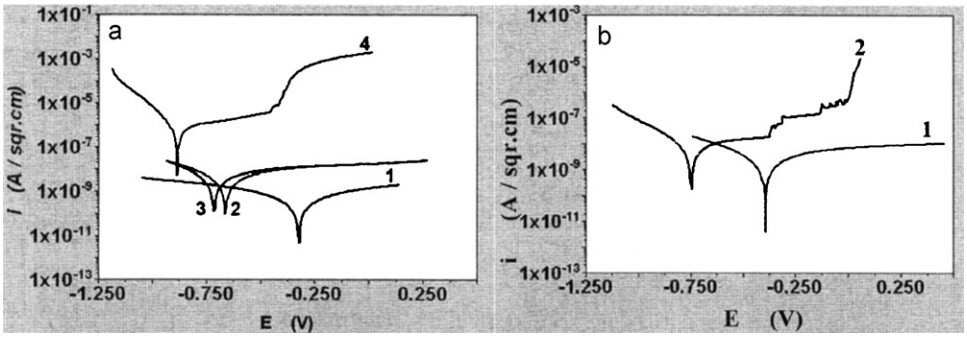

Fig. 1. Potentiodynamic polarization curves of coatings with different $CeCl_3$ content in the matrix. (a) After 24 h; curve 1: 0 wt.%, curve 2: 2 wt.%, curve 3: 4 wt.%, and curve 4: bare alloy; (b) 1500 h of exposure, curve 1: 2 wt.% and curve 2: 4 wt.% $CeCl_3$.

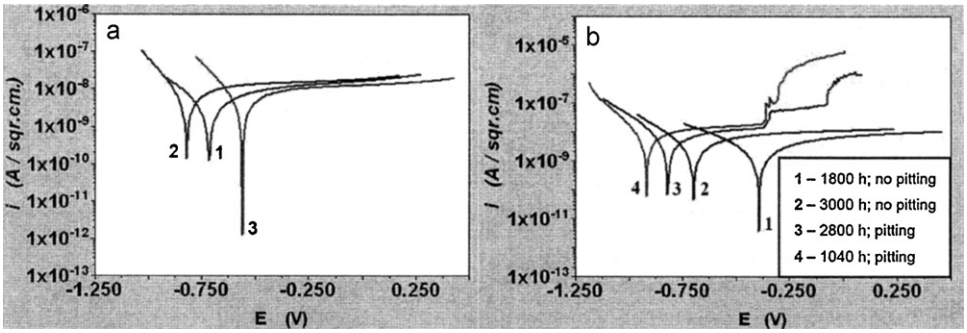

Fig. 2. Potentiodynamic polarization curves. (a) Coatings after 24 h test, constant amount of 4 wt.% $CeCl_3$, at different content of Al_2O_3 nano-particles; curve 1: 0 wt.%, sample I; curve 2: 18 wt.%, sample D; curve 3: 30 wt.%, sample G; (b) tests above 1000 h, samples with 2 wt.% $CeCl_3$ and different content of Al_2O_3, curve 1: 0 wt.%, sample H; curve 2: 8 wt.%, sample A; curve 3: 18 wt.%, sample C; curve 4: 30 wt.%, sample F.

the Nyquist plot only one semicircle was registered. It corresponds to the time constant expressed by a parallel connection between R_{coat} and C_{coat}. In the same plot after the semicircle a slope straight line appears at the lowest frequency region. The slope of this line is predetermined by the ratio $Z'':Z'$, which is a constant value: $n = \Delta Z''/\Delta Z' = \text{const}$. Here Z'' is the imaginary component and Z' is the real component of the impedance, respectively. In the highest frequency region at $\log(f) = 5$ the phase shift is higher than 90°, for all of the EIS spectra. This phenomenon is related to the construction of the corresponding test-cell. The counter electrode was in form of cylinder, whose walls stay in perpendicular direction to the plane of the sample's surface (working electrode).

It is necessary to underline that in case of coatings, containing $CeCl_3$ inhibitor, new $Al_nCl_{(3n-m)}(OH)_m$ interlayer could be formed. This substance is known as an inorganic polymer which possesses typical Keggin's structure. The substance possesses a tendency to form large variety of poly-aluminium complexes [34], as well. In the bulk of this poly-aluminium complex appears a concentration gradient of reactants and products of the corrosion process. These species could be H^+, OH^-, $Al(OH)_4^-$, etc. For example, the tetrahydroxyaluminate ions are product of the following reactions:

$$Al + 3(OH)^- \rightarrow Al(OH)_3 \quad (1)$$

$$Al(OH)_3 + OH^- \rightarrow Al(OH)_4^- \quad (2)$$

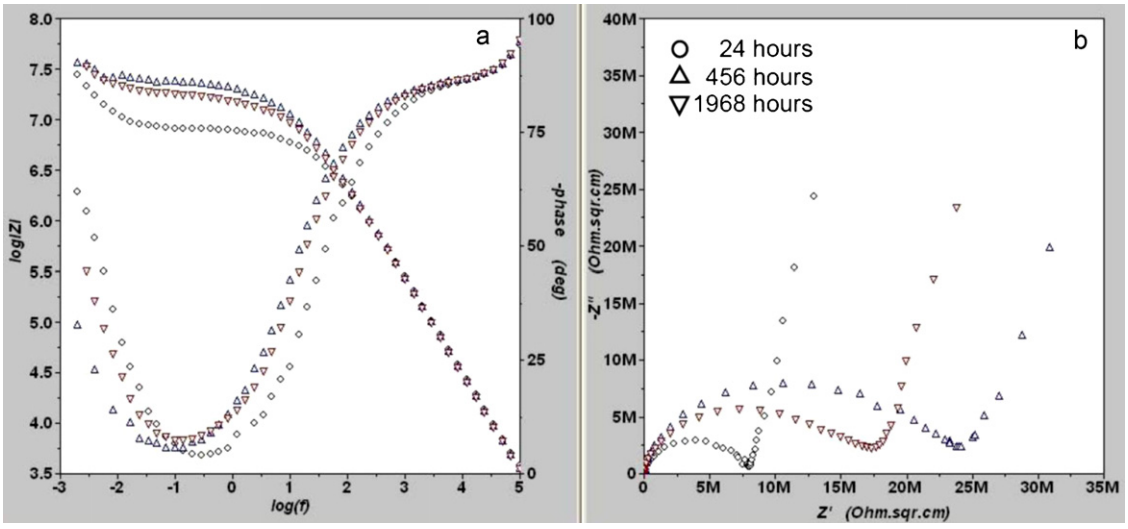

Fig. 3. Impedance spectra in Bode (a), and Nyquist (b) plots of coating A after different exposure times.

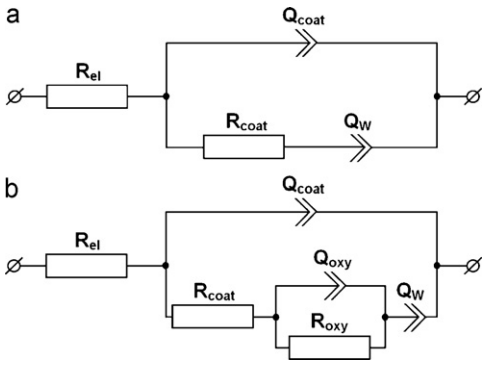

Fig. 4. Equivalent schemes, used for the impedance modeling. R_{el}, R_{coat}, R_{oxy}, resistances of: electrolyte; electrolyte in the pores of the pre-treatment; the oxide layer. Q_{coat} and Q_{oxy} are constant phase elements, which correspond to the capacities of the coatings and the intermediated oxide layer. Q_W is constant phase element which corresponds to the diffusion.

The corrosion of the substrate (AA2024), protected by the synthesised coatings with an addition of $CeCl_3$, is entirely driven by the diffusion kinetics. It was established that the slope of the straight line at the lowest frequency part of the spectra, presented in Nyquist plot is situated in the range between $n = 0.78$ and 0.90 for all spectra. This value is higher than $n = 0.5$, typical for the Warburg's diffusion impedance. It is obvious that the diffusion process in the present case deviates from the ideal Fick's law for linear semi-infinite diffusion.

We have performed structural impedance modeling to evaluate quantitatively the coatings properties. It was carried out by a fitting procedure of the experimental spectra according to an appropriate equivalent scheme. Fig. 4 shows the equivalent schemes, used in the present study. The spectra of the specimens with higher $CeCl_3$ content, after extended exposure, were composed by a semi-circle with small radius and elongated straight line in the lowest frequency part. For their fitting the equivalent circuit, represented on Fig. 4(a) was used, while for all of the rest cases the equivalent scheme on Fig. 4(b) was applied.

The constant phase elements (Q) were used instead of pure capacitances (C) in both of the schemes. Similar substitution is necessary, in all cases, when the phase shift (φ) is smaller than 90°. Like the capacitance, the constant phase element depends on the frequency, according to Eq. (3):

$$Q = Y_o^{-1}(j\omega)^{-n}, \quad (3)$$

where Y_o and n are the frequency independent constants, ω is an angular frequency. It is necessary to mark that for the n values between $0.8 < n < 1$, the constant Y_o has the significance of capacitance and may be measured in Farads. On the base of the obtained Y_o and n values the calculations of the pure capacitance were carried out, applying Eq. (4):

$$C = Y_o\omega_o^{n-1}, \quad (4)$$

where ω_o is the value of the angular frequency, which corresponds to the maximum value of the imaginary component of the impedance for the corresponding time constant.

Another special feature of the equivalent circuits used (Fig. 4) is the substitution of the Warburg element – W, by the corresponding constant phase element – Q_W. This substitution is permitted in the cases when the diffusion is deviated from the ideal Fick's law [35]. Satisfying the level of reliability, $\chi^2 = (4.7–4.9) \times 10^{-3}$ was achieved, when the unique observable semicircle was fitted via two overlapped time-constants ($\tau_1 = R_1C_1$ and $\tau_2 = R_2C_2$), with identical values of the capacitance ($C_1 \sim C_2$). In that case the obtained values for the resistances (R_1 and R_2) of each time-constant could be assigned to the resistance of the coating (R_{coat}), and of the intermediate oxide film (R_{oxy}).

Fig. 5 illustrates the correlation between the experimental spectra (dashed lines) and the fitted spectra (continuous line) for coating C (see Table 1). The equivalent circuits in Fig. 4 have been used for the fitting procedure. The same fitting procedure was used for the spectra of each sample, in order to acquire values for every impedance parameter of the respective sample.

The values obtained and their developments within the exposure time are shown in Table 2. The data show the presence of high values for the resistance of the electrolyte in the pores of the coating (R_{coat}), in range of 10^6 to 10^7 Ω cm^2, combined with a very low capacitance $C_{coat} = 10^{-9}$ to 10^{-10} F/cm^2. Similar values are typical for the coatings with remarkable protective ability [5]. After an extended exposure time crevice corrosion appears on the surface coating. This appearance coincides with sharp change in the shape of the corresponding impedance spectrum. In that case the diffusion limits which control the corrosion process stop to drive it. Simultaneously a new time constant appears in the low frequency region of the spectrum, which reveals corrosion of the substrate (see Fig. 6). The changed spectra, showing the substrate's corrosion, did not undergone next fitting procedures. It was not necessary, because their fitting is not related to the aims of present research. The influence of the coatings over kinetics of the self-healing effect will be an object of further investigations.

The influence of the composition over the resistance R_{coat} of the electrolyte enclosed in the pores of the coatings and its evolution within the exposure time is illustrated in Fig. 7. The values of R_{coat} were followed within the time, until the pitting appeared. The figure reveals that the sample H and I (Table 1) prepared by direct introduction of inhibitor into the hybrid matrix, show the highest values of R_{coat}, but they are not stable for longer periods of exposure. The pitting nucleation appears earlier, when the $CeCl_3$ content is much higher. For sample I with 4 wt.% $CeCl_3$ (see Fig. 7(b)) the pitting appeared after 1500 h, while for specimen H with 2 wt.% $CeCl_3$ inhibitor, no pitting was observed, even after 2000 h of exposure.

The indirect introducing of the inhibitor by Al_2O_3 nano-particles causes a decrease of R_{coat}. We suggest that this effect is caused by an easier penetration of electrolyte through the porous aggregations of Al_2O_3 which stimulates pathway formation across the coating. This negative effect of the nano-particles introduction is compensated by their positive effect on the durability of the coatings. It can be seen in Fig. 7 that the durability remarkably increases for samples with 8 and 18 wt.% of Al_2O_3 nano-particles in comparison to non-doped ones. It was established that for coatings with 2 wt.% $CeCl_3$, doped with 8 wt.% and 18 wt.% Al_2O_3, no pitting was observed, even after 3000 h. However, the durability is strongly decreased, when the nano-particle's concentration is too high. It is necessary to mark that for composition F (2 wt.% $CeCl_3$ and 30 wt.% Al_2O_3) pitting was already proved after 650 h of exposure. In addition for sample G, containing 4% of $CeCl_3$ and 30% nano-particles, pitting spots have already appeared after the initial 240 h time of exposure. Simultaneously, the same sample showed a sharp increase of R_{coat}. An explanation for this fact is an obstruction of the hollow structures of the nano-particles by corrosion products, which structure is probably similar to the described in [34].

Fig. 8 shows the influence of the composition and exposure time of the coatings on their capacitance. Evidently, the coatings possess stable capacitance C_{coat} values, which are not notably influenced by the exposure time. This is because all pores are filled with water shortly after the immersion in electrolyte and therefore, the values of the relative dielectric permeability (ε_r), of the electrolyte filled coatings is near to those of water (equal to 60–90). Also, the electrolyte invasion did not lead to a significant swelling of the coating which would be displayed by an increase of the capacitance.

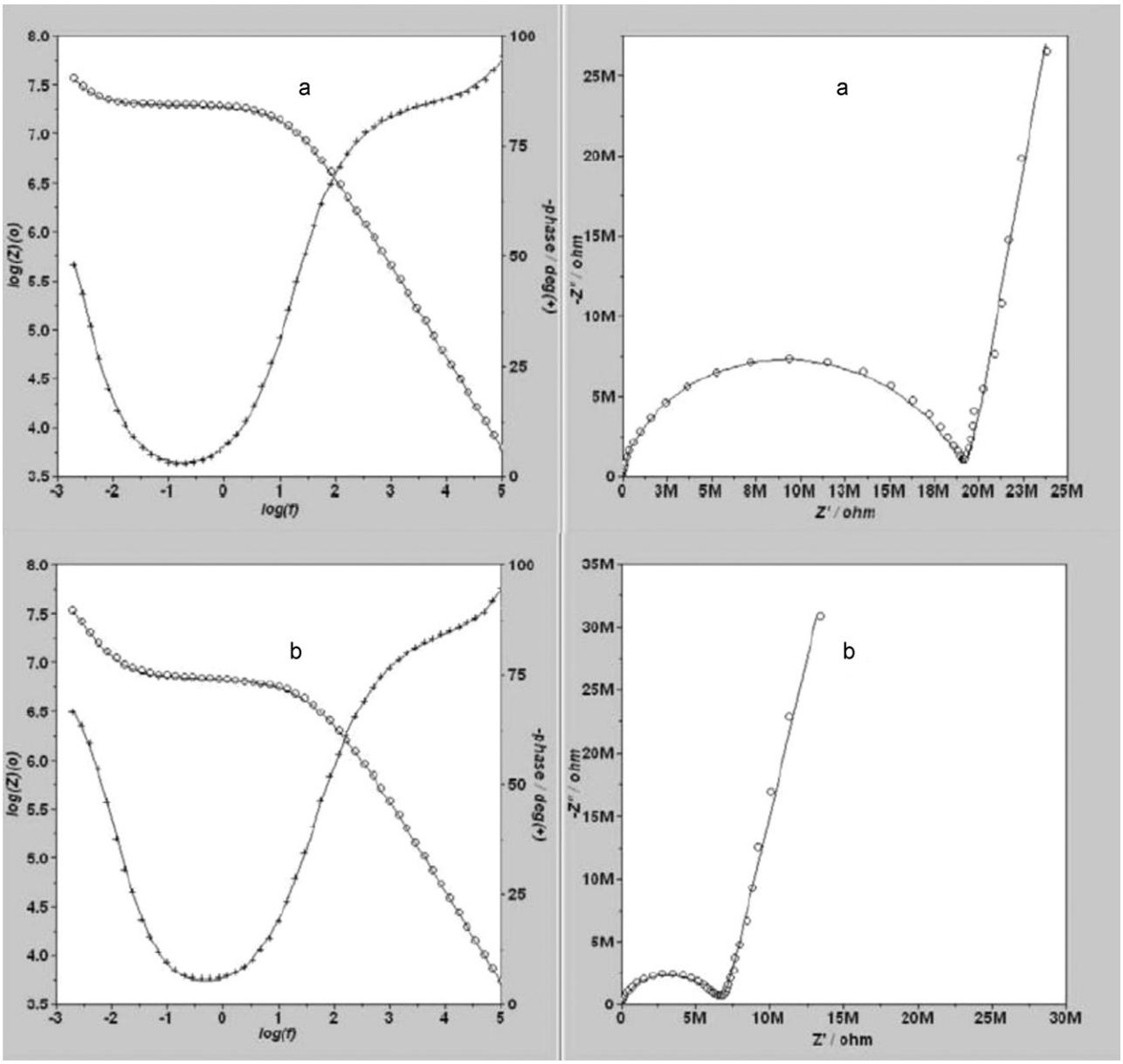

Fig. 5. Correlation between experimental (with dashed lines) and the fitted (continuous lines). spectra for sample C. (a) After 72 h of exposure; (b) after 2800 h of exposure to the corrosive medium.

The influence of the composition on the capacitance of the coatings could be interpreted having in account the formula for the specific capacity C of a flat capacitor:

$$C = \frac{\varepsilon_0 \varepsilon_r}{d}, \quad (5)$$

where $\varepsilon_0 = 8.85 \times 10^{-12}$ F/m; ε_r is relative dielectric permeability and d the distance between the plates of the capacitor.

The coatings H (with 2% $CeCl_3$) and I (with 4% $CeCl_3$) possess the lowest values of the capacitance. The reason for this fact is that after the introduction of a salt whose aqueous solutions are electric conductive, their ε_r value strongly decreases. The decrease is more remarkable, when the amount of $CeCl_3$ in the matrix is higher.

It is complicated to predict how ε_r will change, when the inhibitor is introduced by nano-containers. In that case, it could

Table 2
Numerical values of the impedance parameters for sample C and their evolution within the exposure time.

Time (h)	R_{coat} ($\times 10^6\ \Omega\,cm^2$)	R_{oxy} ($\times 10^6\ \Omega\,cm^2$)	C_{coat} ($\times 10^{-10}$ F/cm^2)	C_{oxy} ($\times 10^{-10}$ F/cm^2)	Q_W	
					Y_o ($\times 10^{-4}$)	n
24	9.01 ± 0.60	9.74 ± 0.63	4.47 ± 0.07	7.11 ± 0.63	1.72 ± 0.04	0.87
384	7.39 ± 0.71	14.57 ± 0.74	4.52 ± 0.10	4.85 ± 0.34	1.75 ± 0.02	0.90
816	3.55 ± 0.60	8.42 ± 0.63	4.55 ± 0.12	4.92 ± 0.49	1.70 ± 0.03	0.88
1392	2.55 ± 0.51	9.31 ± 0.69	4.65 ± 0.17	5.04 ± 0.50	1.54 ± 0.03	0.87
1872	2.87 ± 0.80	12.98 ± 0.86	4.79 ± 0.18	5.24 ± 0.52	1.40 ± 0.04	0.87
2904	1.68 ± 0.04	6.15 ± 0.24	5.07 ± 0.23	5.93 ± 0.30	1.41 ± 0.10	0.81

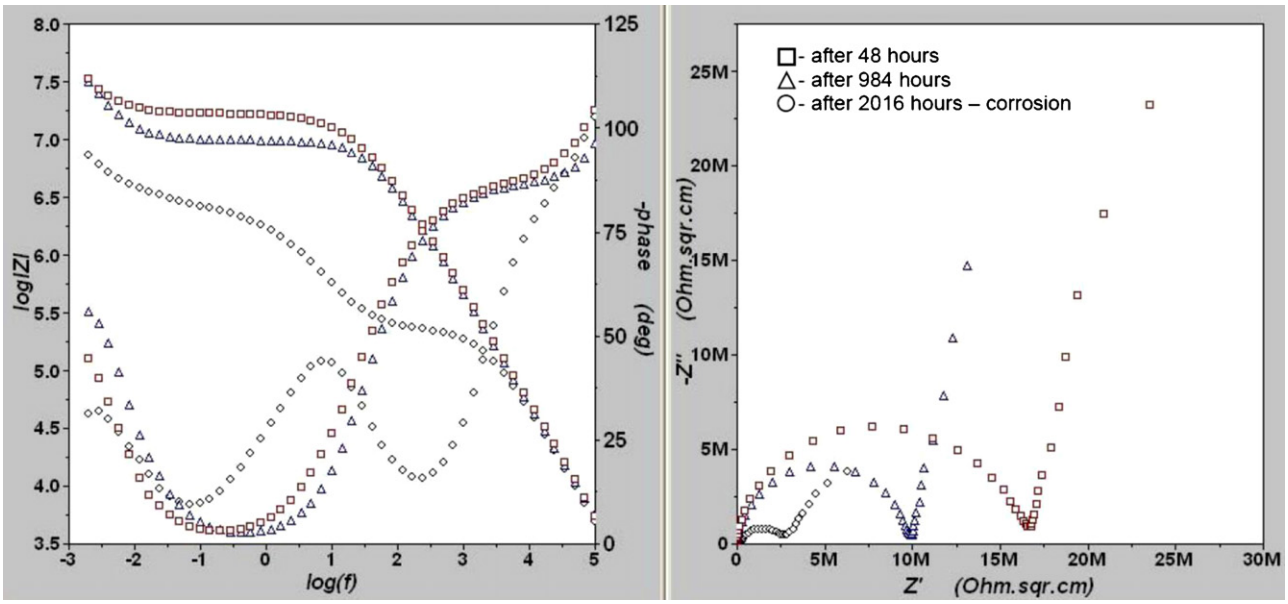

Fig. 6. Development of the impedance spectra of coating I until appearance of substrate corrosion.

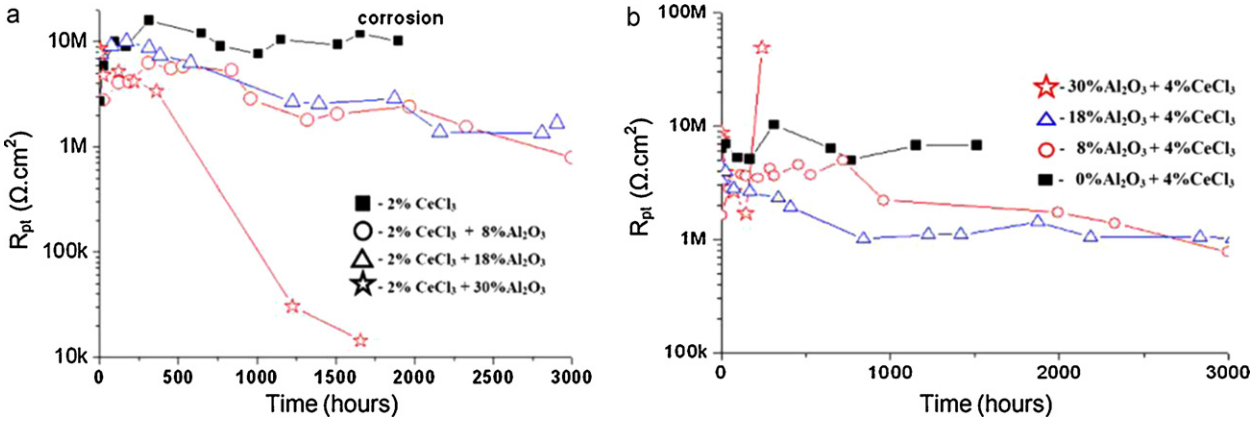

Fig. 7. Dependence of R_{coat} versus exposure time. (a) For samples with 2 wt.% $CeCl_3$; (b) for samples with 4 wt.% $CeCl_3$.

be consider that ε_r does not change significantly, for variation of nano-particles amount in the hybrid matrixes. Then, according to formula (5), the capacitance will depend only on the thickness d of the coatings. In fact the coatings A (2 wt.% $CeCl_3$, and 8 wt.% Al_2O_3) and B (4 wt.% $CeCl_3$, and 8 wt.% Al_2O_3), possess the highest capacitance, as it could be seen from Fig. 8, because that they are the thinnest samples (see Table 1).

3.3. Neutral salt spray test measurements

The results, acquired by means of SST are represented in Table 3. The first numeric column of this table shows the time expired until appearance of the first pitting spot on random sample from the respective group of a given coating composition. The second numerical column contains data for the time expensed until the number of pitting spots began at least 10. In the third column is

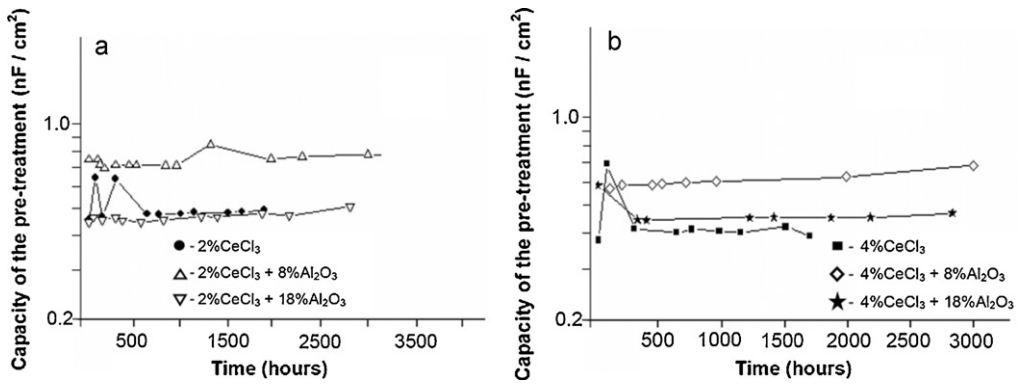

Fig. 8. Dependence of C_{coat} versus exposure time. (a) For samples with 2 wt.% $CeCl_3$; (b) for samples with 4 wt.% $CeCl_3$.

Table 3
Behaviour of the different samples during exposure to the neutral salt spray test.

Samples	First pits (h)	>10 pits (h)	Removal from the test after (h) (first/last specimen)
Sample A – 2 wt.% $CeCl_3$–8 wt.% Al_2O_3	1000	2000	3000/3660
Sample C – 2 wt.% $CeCl_3$–18 wt.% Al_2O_3	500	500	1170/1170
Sample F – 2 wt.% $CeCl_3$–30 wt.% Al_2O_3	170	340	3000/3000
Sample B – 4 wt.% $CeCl_3$–8 wt.% Al_2O_3	170	500	500/2160
Sample D – 4 wt.% $CeCl_3$–18 wt.% Al_2O_3	340	2160	3660/3660
Sample G – 4 wt.% $CeCl_3$–30 wt.% Al_2O_3	340	670	3000/3000

presented the test time, for the first and the last sample from the corresponding group. This column gives a real image of the reproducibility of the results for the coatings object of SST study. From this table could be seen, that the best behaviour, from the point of view of corrosion durability, is observed for the coatings A and C (2 wt.% $CeCl_3$ and 8 wt.%; 18 wt.% Al_2O_3), while the worst results belong to the coatings with the highest content of nano-particles: i.e. samples F (2 wt.% $CeCl_3$ and 30 wt.% Al_2O_3), and G (4 wt.% $CeCl_3$ and 30 wt.% Al_2O_3), respectively. This fact completely confirms the results of the EIS measurements (see Fig. 7), regarding the samples F and, G, but it does not correspond for the rest three coatings. The available explications could be given, having in account the significant differences of the conditions of execution of the both of tests. For SST test the fluid in contact with the samples permanently exchanges, and as result, the cerium salt leaches more quickly. Besides, because of the more than 10 times higher concentration of NaCl used for SST, the corrosion processes start earlier than in EIS measurements.

The results, obtained by SST, show that the optimal correlation between these parameters is achieved at a weight ratio of inhibitor to the nano-particles of 1:4 (coatings A and D). The coating D, shows preferable characteristics, compared to coating A, because for nano-particles content of 18 wt.%, we have achieved the highest rate of reinforcement.

4. Conclusions

Sol–gel hybrid oxysilane coatings with additions of pure $CeCl_3$ and $CeCl_3$-filled Al_2O_3 nano-containers have been deposited on AA2024-T3 aluminium alloy. Their corrosion-protective ability and durability in 0.05 M NaCl were evaluated by the linear voltammetry (LVA) and the electrochemical impedance spectroscopy (EIS) methods.

The synthesised inorganic–organic hybrid coatings without any doping agents possess remarkable barrier ability and durability. These coatings reveal high barrier resistance $R_{coat} = 10^6$ to $10^7\,\Omega\,cm^2$ and extraordinary low capacitance $C = 10^{-9}$ to $10^{-10}\,F/cm^2$. After the introduction of inhibitor, directly into the into the hybrid matrix, these parameters suffer deterioration. When the inhibitor is incorporated in the nano-particles, the durability improves remarkably. The highest durability possess coatings, with a weight ratio inhibitor: nano-particles equals 1:4. It was established that the coatings containing 2 wt.% $CeCl_3$ and 8 wt.% Al_2O_3 nano-containers could retain into the corrosive medium more than 3000 h before any corrosion appeared. As a result of analysis of the impedance spectra and the structural impedance modeling it is concluded that the substrate corrosion for these coatings passes the diffusion control, where the diffusion process deviates from the ideal low of Fick for non-stationary diffusion.

The hybrid oxysilane coatings with $CeCl_3$, incorporated in porous aggregates of Al_2O_3 nano-containers, provide reliable and durable protection of the AA2024 alloy. They are able to be used as perspective alternative of the toxic chromium-containing coatings.

Acknowledgements

The financial support from EC-6fp Integrated project MULTI-PROTECT and from the Bulgarian NSF, contract DVU-02/102 are highly appreciated. The authors are grateful to Assoc. Prof. Dr. I. Nenov for the useful discussion done.

References

[1] M.L. Zheludkevich, R. Serra, M.F. Montemor, M.G.S. Ferreira, Electrochem. Commun. 7 (2005) 836.
[2] M.L. Zheludkevich, I.M. Salvado, M.G. Ferreira, J. Mater. Chem. 15 (2005) 5099.
[3] G. Gusmano, G. Montesperelli, M. Rapone, G. Padeletti, A. Cusmà, S. Kaciulis, A. Mezzi, R. Di Maggio, Surf. Coat. Technol. 201 (2007) 5822.
[4] G. Kong, L. Jitang, W. Haijiang, J. Rare Earth 27 (2009) 164.
[5] W. Trabelsi, P. Cecilio, M.G.S. Ferreira, M.F. Montemor, Prog. Org. Coat. 54 (2005) 276.
[6] J. Gallano, A. Duran, J. de Damborenea, Corros. Sci. 46 (2004) 795.
[7] R. Surrlit, T. Koch, U. Schubert, Corros. Sci. 49 (2007) 3015.
[8] D. Raps, T. Hack, J. Wehr, M.L. Zheludkevich, A.C. Bastos, M.G.S. Ferreira, O. Nuyken, Corros. Sci. 51 (2009) 1012.
[9] H. Guan, R.G. Buchheit, Corrosion 60 (2004) 284–296.
[10] C. Wang, F. Jiang, Corrosion 60 (2004) 237.
[11] Q.S. Yu, H.K. Yasuda, Prog. Org. Coat. 52 (2005) 217.
[12] L.E.M. Palomino, I.V. Aoki, H.G. De Melo, Electrochim. Acta 51 (2006) 5943.
[13] A. Duran, Y. Castro, M. Aparicio, A. Conde, J. de Damborenea, Int. Mater. Rev. 52 (2007) 175.
[14] E.A. Starke, J.T. Staley, Prog. Aerospace Sci. 32 (1996) 131.
[15] K.A. Yasakau, M.L. Zheludkevich, S.V. Lamaka, M.G.S. Ferreira, J. Phys. Chem. B 110 (2006) 5515.
[16] P. Camperstini, H. Terryn, A. Hovestad, J.H. Wit de, Surf. Coat. Technol. 176 (2004) 365.
[17] M.L. Zheludkevich, K.A. Yasakau, S.K. Poznyak, M.G.S. Ferreira, Corros. Sci. 47 (2005) 3368.
[18] I.T.E. Fonseca, N. Lima, J.A. Rodrigues, M.I.S. Pereira, J.C.S. Salvador, M.G.S. Ferreira, Electrochem. Commun. 4 (2002) 353.
[19] P. Campestrini, E.P.M. van Westing, H.W. van Rooijen, J.H. de Wit, Corros. Sci. 42 (2000) 1853.
[20] H. Schmidt, S. Langenfeld, R. Nass, Mater. Des. 18 (1997) 309.
[21] M.L. Zheludkevich, R. Serra, M.F. Montemor, K.A. Yasakau, M. Salvado, M.G.S. Ferreira, Electrochim. Acta 51 (2005) 208.
[22] S. Kozhukharov, G. Tsaneva, V. Kozhukharov, J. Gerwann, M. Schem, T. Schmidt, M. Veith, J. Univ. Chem. Technol. Met. 43 (2008) 73.
[23] T. Schmidt, P.W. Oliveira, M. Mennig, H. Schmidt, J. Non-Cryst. Solids 353 (2007) 2826.
[24] R. Di Maggio, S. Rossi, L. Fedrizzi, P. Scardi, Surf. Coat. Technol. 89 (1997) 292.
[25] A.J. Aldykiewicz Jr., A.J. Davenport, H.S. Isaacs, J. Electrochem. Soc. 143 (1996) 147.
[26] S.A. Hayes, P. Yu, T.J. O'Keefe, J.O. Stoffer, J. Electrochem. Soc. 149 (2002) C623–C630.
[27] M. Schem, T. Schmidt, H. Caparrotti, M. Aslan, M. Veith, M. Wittmar, in: Proc. Eurocorr 2008, Paper 1034, Edinburgh, UK, September 7–11, 2008.
[28] M. Schem, T. Schmidt, J. Gerwann, M. Wittmar, M. Veith, G.E. Thompson, I.S. Molchan, T. Hashimoto, P. Skeldon, A.R. Phani, S. Santucci, M.L. Zheludkevich, Corros. Sci. 51 (2009) 2304.
[29] B.B. Damaskin, O.A. Petrijy, Introduction into the Electrochemical Kinetics, Higher School, 1980, p. 52.
[30] S. Koka, A. Shi, J.S. Ullet, Proc. Conf. "S & K Technologies", Dyton, OH, USA, May 12, 2004.
[31] B.A. Boukamp, J. Electrochem. Soc. 142 (1995) 1885.
[32] F. Mansfeld, Corrosion 32 (1976) 143.
[33] M. Schem, T. Schmidt, H. Caparrotti, M. Wittmar, M. Veith, in: L. Fedrizzi (Ed.), Self-Healing Properties of New Surface Treatments (European Federation of Corrosion), Maney Publishing, UK, 2010, ISBN 1906540365.
[34] J. Rowsell, L.F. Nazar, J. Am. Chem. Soc. 122 (2000) 3777.
[35] Z. Stoynov, B. Grafov, B. Savova-Stoynova, V. Elkin, Electrochemical Impedance, Nauka, Moscow, 1991, pp. 61–62 (in Russian).